AWARD NUMBER: W81XWH-12-1-0286

TITLE: Improving the Diagnostic Specificity of CT for Early Detection of Lung Cancer: 4D CT-Based Pulmonary Nodule Elastometry

PRINCIPAL INVESTIGATOR: Peter. G. Maxim, PhD

CONTRACTING ORGANIZATION: Stanford University
Menlo Park, CA 94025-3434

REPORT DATE: October 2015

TYPE OF REPORT: Final

PREPARED FOR: U.S. Army Medical Research and Materiel Command
Fort Detrick, Maryland 21702-5012

REPORT DOCUMENTATION PAGE

Form Approved
OMB No. 0704-0188

1. REPORT DATE	2. REPORT TYPE	3. DATES COVERED
October 2015	**Final**	15 July 2012 – 14 July 2015

4. TITLE AND SUBTITLE

Improving the Diagnostic Specificity of CT for Early Detection of Lung Cancer 4D CT-Based Pulmonary Nodule Elastometry

5a. CONTRACT NUMBER
W81XWH-12-1-0286

5b. GRANT NUMBER

5c. PROGRAM ELEMENT NUMBER

6. AUTHOR(S)
Peter G Maxim, PhD,
Billy W Loo, MD, PhD

E-Mail: pmaxim@stanford.edu

5d. PROJECT NUMBER

5e. TASK NUMBER

5f. WORK UNIT NUMBER

7. PERFORMING ORGANIZATION NAME(S) AND ADDRESS(ES)

STANFORD UNIVERSITY
450 SERRA MALL
STANFORD, CA 94305-2004

8. PERFORMING ORGANIZATION REPORT NUMBER

9. SPONSORING / MONITORING AGENCY NAME(S) AND ADDRESS(ES)
U.S. Army Medical Research and Materiel Command
Fort Detrick, Maryland 21702-5012

10. SPONSOR/MONITOR'S ACRONYM(S)

11. SPONSOR/MONITOR'S REPORT NUMBER(S)

12. DISTRIBUTION / AVAILABILITY STATEMENT
Approved for Public Release; Distribution Unlimited

13. SUPPLEMENTARY NOTES

14. ABSTRACT In this study we propose to develop and validate pulmonary nodule elastometry imaging, a method complementary to CT that has the potential to increase the specificity of screening for early detection of lung cancer. We propose to address the need for the greater specificity in lung cancer screening by characterizing a mechanical property of pulmonary lesions, specifically pulmonary nodule (PN) elasticity, in addition to standard anatomic features. We hypothesize that malignant and benign PN can be distinguished more specifically by different elasticities determined from 4D CT images. The specific aims of the study were the development of pulmonary nodule elastometry algorithms based on deformable image processing of 4D CT images and their validation in an animal model and in a retrospective review of over 200 4D CT scans from patients with small malignant pulmonary nodules previously treated with radiation in our department. We have successfully developed algorithms, and in a first validation we have demonstrated proof of principles that elastometry can distinguish malignant PNs from surrounding lung tissue (a manuscript is in preparation). The validation in animal models and the retrospective analysis of the human data is ongoing.

15. SUBJECT TERMS: pulmonary nodule elastometry, 4DCT, deformable image registration, Jacobian, lung cancer, lung cancer screening

16. SECURITY CLASSIFICATION OF:			17. LIMITATION OF ABSTRACT	18. NUMBER OF PAGES	19a. NAME OF RESPONSIBLE PERSON
a. REPORT	b. ABSTRACT	c. THIS PAGE			USAMRMC
U	U	U	UU	32	19b. TELEPHONE NUMBER *(include area code)*

Table of Contents

Contract number: W81XWH-12-1-0286

Title: Improving the Diagnostic Specificity of CT for Early Detection of Lung Cancer: 4D CT-Based Pulmonary Nodule Elastometry

Principal Investigator: Peter G Maxim, PhD

Introduction:

In this project we are addressing a shortcoming of existing lung cancer screening methods by developing a CT based method of characterizing a mechanical property of pulmonary lesions, specifically tissue elasticity (stiffness) that should have a higher specificity than purely anatomic low-dose CT. It is the aim of the proposed study to decrease the false positive rate of CT screening by analyzing the mechanical properties of suspiciously appearing tissue during CT screening. We hypothesize that malignant pulmonary nodules are less elastic (stiffer) than benign nodules and that this difference in elasticity can be used to differentiate cancerous from benign nodules, which would help to decrease the false positive rates of CT screening. A measure of elasticity can be derived from high-resolution 4-dimensional computed tomography (4D CT) using deformable image registration algorithms. Unlike conventional 3D CT imaging that results in a static image of the scanned anatomy, 4D CT incorporates also the temporal changes of the anatomy caused by respiratory motion, yielding a CT 'movie' that allows the evaluation of tumor motion and the calculation of the elasticity.

Body:

Specific Aim 1. Development of deformable image algorithms for processing the 4D CT images to determine the elasticity of malignant and benign pulmonary nodules. *(**Dr. Maxim**, Tasks 1, months 1 – 8)*

Task 1. Development of the software for deformable image registration, analysis of the DVF and the calculation of the elasticity parameter (Matlab).

*The software will be developed using the mathematical package Matlab (The Mathworks Inc., Natick, MA). Two deformable image registration algorithms will be used (DIR^{vol} and a method based on optical flow, DIR^{OF}). The resulting displacement vector fields will be analyzed and an elasticity parameter for the pulmonary nodules will be calculated (**Dr. Maxim**, months 1 – 8).*

Status (Task 1):

A manuscript describing our algorithm and its validation was accepted for publication in 'Radiotherapy and Oncology'and is attached to this report.

Specific Aim 2: Validate our method in rat models of human lung cancer and benign inflammatory lesions. *(**Dr. Maxim**, Tasks 2-4, months 3 – 24)*

Task 2. Preliminary experiments: Establish optimal protocol for the benign pulmonary model (granulomatous inflammation) and study growth kinetics.

*2a. Purchase animals: Rowett rats, A549 and SK-MES-1 cells from American Tissue Culture Collection (ATCC), carbon nanotubes (catalogue number 900–1501, lot GS1801), SES research (Houston, TX) and necessary culturing media. (**Dr. Maxim**, months 1-3)*

*2b. Inoculate 15rats (Rowett nude rats) with carbon nanotubes and follow with serial MicroCT measurements to study growth kinetics to establish the time for nodule development to reach desired size. (**Dr. Maxim**, 15 rats total, months 3 – 6)*

Task 3. Grow orthotopic model of lung cancer and benign lesions and follow with serial MicroCT imaging: preliminary experiments to establish protocol and optimize software

*3a. Inoculate 10 rats with orthotopic human lung cancer cells (A549, left lung) and carbon nanotubes (right lung) (**Dr. Maxim**, months 7-9)*

*3b. Acquire CT images at peak-inhale and peak-exhale using a small animal ventilator (**Dr. Maxim**, month 9-10)*

*3c. Analyze CT images and derive elasticity parameter and optimize software if necessary. (**Dr. Maxim**, month 10)*

Task 4. Grow orthotopic model of lung cancer and benign lesions and follow with serial MicroCT imaging, analyze data

*4a. Inoculate remaining 40 rats (A549 cells, left lung in Rowett nude rats) and follow with CT imaging at peak-inhale and peak-exhale (**Dr. Maxim**, months11-13)*

*4b. Perform simplified analysis: Delineate malignant and benign pulmonary nodules and measure volumes at peak-inhale and peak-exhale. Derive elasticity parameter based on the ratio of the volumes. (**Dr. Maxim**, months 14-15)*

*4c. Analyze acquired CT images and derive elasticity parameter by analyzing the displacement vector fields and perform statistical analysis. (**Dr. Maxim**, months 16-18)*

*4d. Repeat experiments and analysis with second cancer cell line (SK-MES-1), 50 Rowett rats, (**Dr. Maxim**, months 18-23)*

*4e. Publish animal study results (**Dr. Maxim**, month 24)*

Status (Tasks 2, 3, 4): Prolonged repairs on the GE-MicroCT scanner have delayed our proposed experiments, however the defects were fixed and we were able to acquire the proposed 4DCT images and perform the analysis.

Figure 1: Position of mouse with pressure belt in CT scanner.

Figure 1 shows a mouse placed in the CT scanner with the pressure sensing belt around its chest that provided the respiratory signal to the scanner.
Figure 2 shows a typical respiratory trace and and a sagittal CT image overlay of acquisitions acquired at maximum inhale and exhale, respectively. Pulmonary nodules (benign and malignant) were delineated by Dr. Loo and analyzed as described in the manuscript attached to this report (Negahadar 2014).
We were able to to successfully generate two benign pulmonary nodule models using talc and matrigel. The

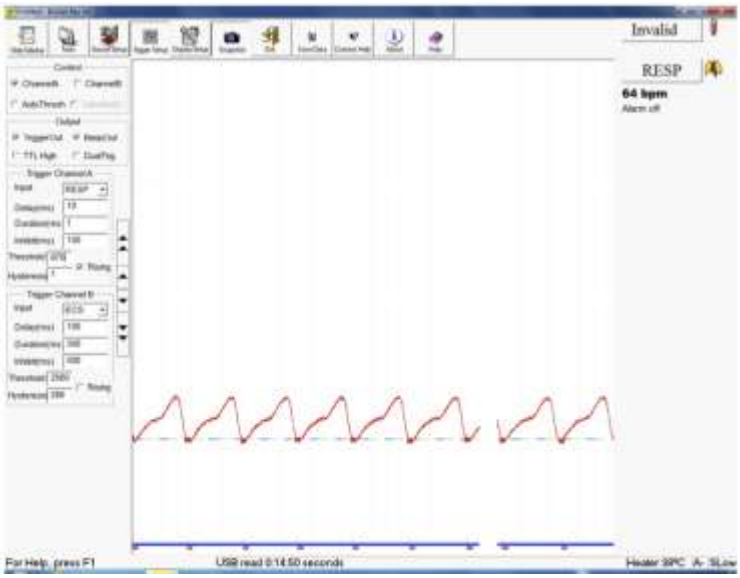

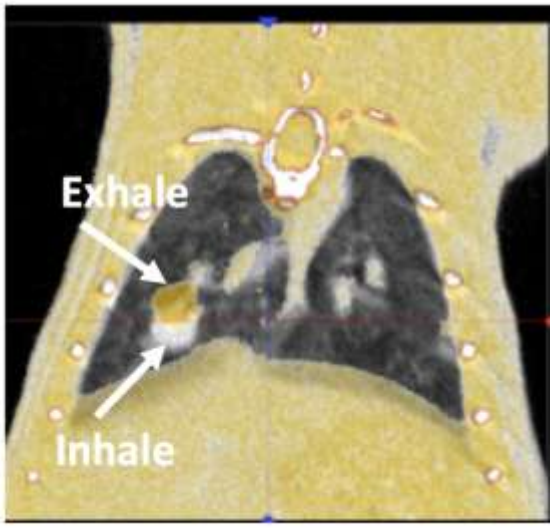

Figure 2: Typical respiratory trace used for acquisition of 4DCT images (left). Right, sagittal 4DCT images acquired at maximum inhale and exhale. Arrows point to nodule location within the lung at exptrme tidal breathing volumes.

calculated elasticities for tumors, talc and matrigel are shown in Figure 3, demonstrating that our proposed method can distinguish between tumors (formed by A549 lung cancer cells) and matrigel. There was no statistically difference in elasticity between tumors and talc.

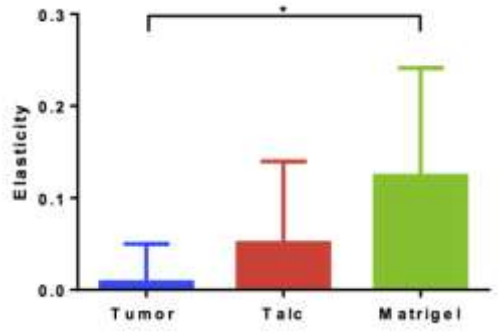

Figure 3: Calculated elasticities of talc, matrigel (benign model)) vs. tumors (A549 lung cancer cells). * indicates statistical difference at $p<0.05$. Error bars indicate SD, N=11.

To validate our results, we performed electronic force microscopy (AFM) on excised samples to verify the elasticities determined by 4DCT image analysis. Figure 4 shows the acquisition technique and derived Young modulus (a metric for tissue elasticity) for tumors, matrigel and lungs. Similar to the elasticity derived from 4DCT image analysis, the Young modulus for tumors was higher for tumors compared to matrigel and lungs, validating the results derived from 4DCT image

analysis. Figure 5 summarizes the results of the AFM derived Young modulus.

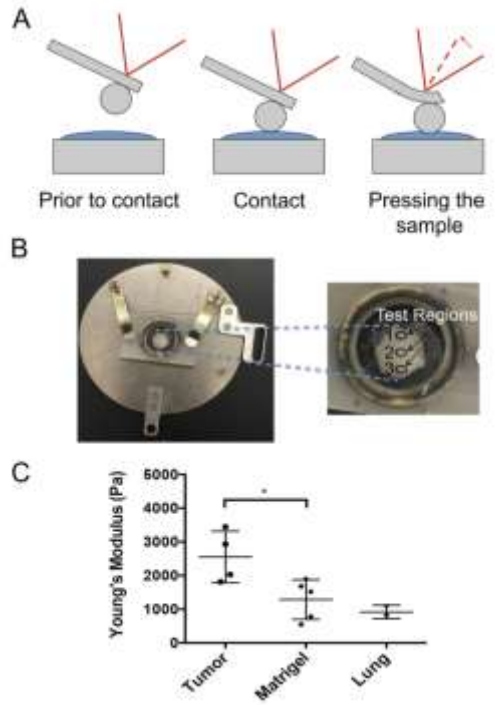

Figure 4: Experimental setup and measurements of the Young modulus via AFM (A and B). Determined Young modulus vis AFM for tumors, matrigel based nodules and lung shows statistical difference between tumors and matrigel, demonstrating the successful ability of 4DCT image based analysis to distinguish malignant vs. benign pulmonary nodules. Errors bars indicate SD, N=4

In summary, we have demonstrated that pulmonary nodule elasticities derived from 4DCT images are able to distinguish benign from malingnants nodules. The results were verified by mechanical measurments of the Young modulus which correlated well with the elasticities derived by 4DCT.

A draft of a manuscript summarizng our methods, results and aknowledging DoD support, is in its final stages and is attached to this report. The manuscript will be submitted to 'Radiotherapy and Oncology' and will be made available to the DoD as soon as it is accepted.

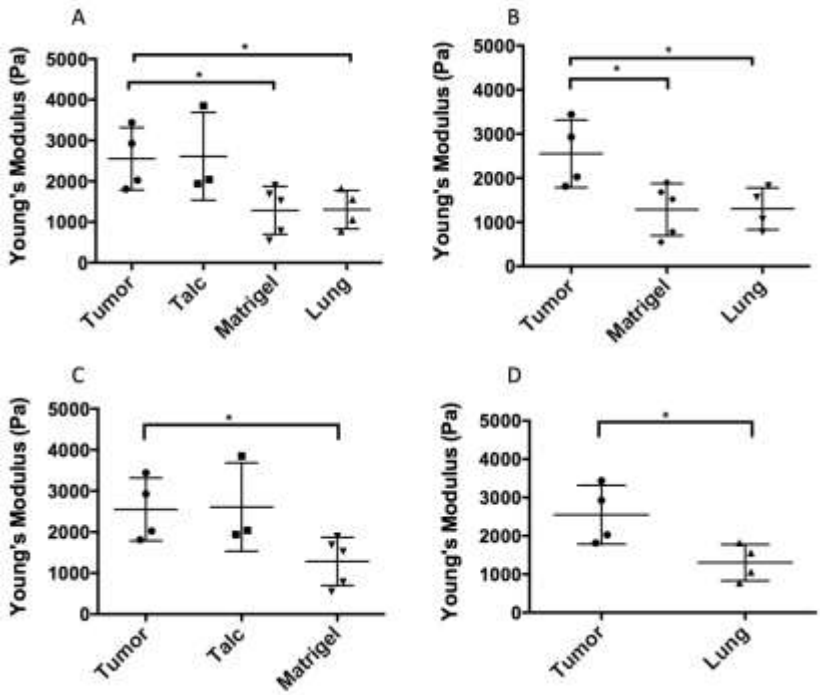

Figure 5: Derived Young modulus via AFM for matrigel, talc and lung tumor models. Statistiacal difference denoted by * is indicated at the $p<0.05$ level. N=4 per group.

Specific Aim 3: Validate our method in a retrospective review of over 200 4D CT scans from patients previously treated in our department. *(**Dr. Loo**, Task 5 months 1 – 20)*

Task 5. Analyze approximately 200 4D CT images from previously treated patients and patients recruited within the funding period.

*5a. De-archive all previously acquired thoracic 4D CT scans and identify suitable patients for the study. Our institutional data (all 4D CT scans) are currently stored on DVD's. Data will be de-archived and suitable lung cancer patients (patients with benign and malignant pulmonary nodules) will be identified. (**Dr. Loo**, months 1 – 3)*

*5b. Identify benign and malignant pulmonary nodules to be included in the analysis and delineate nodules at each respiratory phase. (**Dr. Loo**, month 4)*

*5c. Perform simplified analysis by calculating the ratio of the volumes with respect to peak-inhale. (**Dr. Loo**, months 5-8)*

*5d. Analyze all 4D CT images and derive elasticity parameter by analyzing the displacement vector fields and perform statistical analysis (**Dr. Loo**, months 9-15)*

*5e. Analyze data from new patients acquired during the award period (**Dr. Loo**, months 15-18).*

*5f. Publish human study results (**Dr. Loo**, months 19-20)*

Status (Task 5): We continue to de-archive and analyze more patients. We have identified several patients with benign nodules (in addition to malignant nodules that were treated in our department). From those patients with benign nodules, 30% showed strong motion artifacts in 4DCT that aggravated the analysis. 23% of thus far analyzed patients have very small benign nodules. With the acquired CT resolution, the nodules are comprised of a few voxels. Deformable image registration for objects with such few voxels is inaccurate and 'noisy', thus the data will have limited value. Dr. Loo is completing his task and will include the results in his final report.

Key Research Accomplishments:

Our first aim was to develop and validate an automated software package for determining PN elasticity against a manual contouring method, and preliminarily assess its ability to distinguish malignant tissue by comparing the elasticities of malignant PN with those of the lung. This work is now completed and a manuscript detailing the methodology and the results was accepted in 'Radiotherapy and Onclogy' (and included to this report). Using this algorithm, we have demonstrated in a small animal model proof of principle that 4DCT derived pulmonary elasticity is able to distinguish malignant from benign nodule as hypothesized in this proposal. A draft of a manuscript is attached to this report (please see below). Our clinical data has demonstrated proof of principle that elasticity of early stage lung cancer is a significant independent factor for regional recurrence.

Reportable Outcomes:

The following abstracts have been selected for presentation at ASTRO and AAPM:

1. Mohammadreza Negahdar, Billy W Loo, Maximilian Diehn, Lu Tian, Dominik Fleischmann, and Peter G Maxim, *"Automated Tool for Determining Pulmonary Nodule Elasticity to Distinguish Malignant Nodules,"* ASTRO 2014

2. Mohammadreza Negahdar, Billy W Loo, Maximilian Diehn, Lu Tian, Dominik Fleischmann, and Peter G Maxim, "*Comparison of Four Dimensional Computed Tomography (4D CT) versus Breath Hold Images to Determine Pulmonary Nodule Elasticity*", AAPM 2015

The abstracts are included in the 'Supporting Documentation' section.

Conclusion:

We have successfully accomplished the proposed specific aims of our study. First, we have developed a functional software to process and analyze 4DCT images to distinguish malignant and benign PN. This developed algorithm was validated against manual contouring by an expert and published in a peer reviewed journal (attached). We have also demonstrated, in a small animal model, proof of principles that pulmonary nodule elasticities derived from 4DCT images are able to distinguish malignant vs. benign nodules. Our results were verified and validated by mechanical measurements of the Young modulus via AFM.

Our clinical data from patients treated in our department has demonstrated proof of principle that elasticity derived form 4DTC images of early stage non-small cell lung cancer is a significant independent predictor of recurrence involving or mediated by regional nodal metastasis. This knowledge is useful to predict the aggressiveness of early stage lung cancer and may play a role in the selection of treatment options.

In summary, we have demonstrated proof of principles that mechanical properties, such as PN elasticity can be derived from 4DCT images which has the potential to be used as a prognostic factor for tumor aggressiveness and as a screening tool for early stage lung cancer.

Despite setbacks in time because of upgrades of the small animal equipment and some difficulties with the human data, we have successfully accomplished the proposed aims of our study

Supporting Data:

Abstract submitted to the Annual Conference of ASTRO (2014):

Automated Tool for Determining Pulmonary Nodule Elasticity to Distinguish Malignant Nodules

Purpose: To develop and validate an automated method of determining pulmonary nodule (PN) elasticity against a manual contouring method, and preliminarily assess its ability to distinguish malignant tissue by comparing the elasticities of malignant PNs treated with stereotactic ablative radiotherapy (SABR) with those of the lung.

Methods: We analyzed breath-hold images of 30 patients with malignant PNs who underwent SABR in our department. A parametric nonrigid transformation model based on multi-level B-spline guided by Sum of Squared Differences similarity metric was applied on breath-hold images to determine the deformation map. The Jacobian of the calculated deformation map, which is directly related to the volume changes between the two respiratory phases, was calculated. Next, elasticity parameter will be derived by calculating the ratio of the Jacobian of the PN to the Jacobian of a 1cm region of lung tissue surrounding the tumor (E-ROI) as well as the Jacobian of the whole lung (E-Lung).

Results: For the first group of 15 patients we evaluated the volumetric changes of PNs and the lung from the maximum exhale phase to the maximum inhale phase, whereas the reverse was done for the second group of 15 patients. For the first group, mean and standard deviation for E-ROI and E-Lung were 0.91±0.09 and 0.86±0.18, respectively, which was verified by the manual method. For the second group, E-ROI and E-Lung were 1.34±0.27 and 1.57±0.51, respectively. These results demonstrate that the elasticity of the PNs was less than that of the surrounding lung ($p<0.0037$).

Conclusion: We developed an automated tool to determine the elasticity of PNs based on deformable image registration of breath-hold images. The tool was validated against manual contouring. Preliminarily, PN elastometry distinguishes proven malignant PNs from normal tissue of lung, suggesting its potential utility as a non-invasive diagnostic tool to differentiate malignant from benign PN.

Abstract submitted to the Annual Conference of AAPM (2015):

Comparison of Four Dimensional Computed Tomography (4D CT) versus Breath Hold Images to Determine Pulmonary Nodule Elasticity

Purpose: Elasticity may distinguish malignant from benign pulmonary nodules. To compare determining of malignant pulmonary nodule (MPN) elasticity from four dimensional computed tomography (4D CT) images versus inhale/exhale breath-hold CT images.

Methods: We analyzed phase 00 and 50 of 4D CT and deep inhale and natural exhale of breath-hold CT images of 30 MPN treated with stereotactic ablative radiotherapy (SABR). The radius of the smallest MPN was 0.3 cm while the biggest one was 2.1 cm. An intensity based deformable image registration (DIR) workflow was applied to the 4D CT and breath-hold images to determine the volumes of the MPNs and a 1 cm ring of surrounding lung tissue (ring) in each state. Next, an elasticity parameter was derived by calculating the ratio of the volume changes of MPN (exhale:inhale or phase50:phase00) to that of a 1 cm ring of lung tissue surrounding the MPN. The proposed formulation of elasticity enables us to compare volume changes of two different MPN in two different locations of lung.

Results: The calculated volume ratio of MPNs from 4D CT (phase50:phase00) and breath-hold images (exhale:inhale) was 1.00±0.23 and 0.95±0.11, respectively. It shows the stiffness of MPN and comparably bigger volume changes of MPN in breath-hold images because of the deeper degree of inhalation. The calculated elasticity of MPNs from 4D CT and breath-hold images was 1.12±0.22 and 1.23±0.26, respectively. For five patients who have had two MPN in their lung, calculated elasticity of tumor A and tumor B follows same trend in both 4D CT and breath-hold images.

Conclusion: We showed that 4D CT and breath-hold images are comparable in the ability to calculate the elasticity of MPN.

Respiratory-Gated Non-Invasive CT Imaging of Minute Volume Changes in Pulmonary Nodules is Correlated with Physical Measurements of Stiffness

Frederick M Lartey, Ph.D. [*], Marjan Rafat, Ph.D. [*], Mohammadreza Negahdar, Ph.D. [*], Andrey V Malkovskiy, Ph.D. [†], Bonnie Dong, M.D.[*], Lily Sun, M.D. [*], Mei Li, M.D. [*], Timothy Doyle, DPhil. [‡], Jayakumar Rajadas, Ph.D. [†], Edward E Graves, Ph.D. [*], Billy W Loo, M.D. , Ph.D. [*], Peter G Maxim, Ph.D. [*]

Departments of [*]Radiation Oncology, [†]Radiology, and [‡]Pediatrics, Stanford University, Stanford, CA

[†] Biomaterials and Advanced Drug Delivery Laboratory, Cardiovascular Pharmacology Division, Cardiovascular Institute, Stanford University School of Medicine, 1050 Arastradero Road, Palo Alto, CA 94304

Corresponding authors: Peter G. Maxim, Ph.D., Stanford Cancer Center, 875 Blake Wilbur Dr., Stanford, CA 94305. Tel: (650) 724-3018; Fax: (650) 725-8231; E-mail: pmaxim@stanford.edu Billy W. Loo, Jr., M.D., Ph.D., Stanford Cancer Center, 875 Blake Wilbur Dr., Stanford, CA 94305. Tel: (650) 736-7143; Fax: (650) 725-8231; E-mail: bwloo@stanford.edu

Running title: Respiratory-Gated MicroCT and Pulmonary Nodule Volume Changes

Acknowledgement: This study has been supported by Department of Defense LCRP 2011 #W81XWH-12-1-0286.

Conflict of interest: None.

Keywords: Keywords: Pulmonary Nodules; Deformability; Respiratory-gated MicroCT; Lung Cancer, Rats.

Abstract

Background and Purpose: To validate a non-invasive imaging methodology that measures the volume changes of malignant and non-malignant pulmonary nodules (PN) in rats from one respiratory cycle to the next and to correlate the changes in nodule volume to physical measurements of tissue stiffness.

Methods and Materials: We analyzed 3D-CT scans from respiratory-gated MicroCT imaging at extreme tidal volumes (peak inhale and exhale) of 15 rats with PNs from talc (non-malignant) in the right lung, and PNs from either matrigel (non-malignant) or A549 human lung carcinoma cells (malignant) in the left lung. The volumes of PNs in each state were determined and deformability parameters (δ) defined as the absolute value of the volume ratio of the PNs were derived. Physical analysis of the mechanics of the PNs by atomic force microscopy (AFM) was used to establish a correlative relationship with the non-invasive deformability parameter for each nodule.

Results: PNs with varying tissue characteristics were successfully created in 3 rodent models. There was significant correlation (P = 0.0002) between nodule volume changes as determined by respiratory-gated non-invasive CT imaging and the physical stiffness of the PNs determined from AFM measurements.

Conclusion: Minute changes in volume of PNs from the preclinical respiratory-gated CT imaging were shown to correlate with physical measurements of nodule stiffness from AFM. Future goals involve the use of this methodology to distinguish malignant from benign pulmonary nodules in larger animals and humans.

Introduction

Although advances in surgical, radio, and chemotherapeutic interventions in lung cancer have improved the odds of survival, clinical stage at diagnosis remains the major determinant of survival after therapy [1]. Screening for lung cancer with low-dose computed tomography (CT) is a highly sensitive, non-invasive imaging modality that has been used for early detection of the disease [2]. As a diagnostic tool, however, it is limited in its ability to effectively distinguish between malignant and non-malignant pulmonary nodules, resulting in limited specificity.

Various imaging modalities, primarily based on ultrasonic waves and magnetic resonance, have demonstrated differential diagnosis of malignant and benign tumors in breast and liver in response to mechanical excitation (1). The diagnosis is based on differences in trajectory distortion that can detect the subtle changes in ‘stiffness’ between malignant and non-malignant tumors. Since ultrasound imaging is technically challenging for lung tissue, high resolution dynamic CT imaging, in contrast to static morphological imaging, could capture temporal changes, such as deformations and organ motion, and could potentially distinguish between malignant and non-malignant pulmonary nodules.

We hypothesize that different PNs have distinct deformability characteristic patterns that can be derived from dynamic CT images acquired at breath-hold at extreme tidal volumes (peak-inhale and exhale) within each respiratory cycle. The underlying principle proposes that malignant nodules are stiffer relative to the lung and undergo significantly less volumetric changes from one respiratory phase to another. In contrast, the less stiff non-malignant nodules will undergo significantly greater volumetric changes.

This study seeks to demonstrate that the volumetric changes of PNs with varying composition and unique physical characteristics as determined non-invasively by respiratory-gated dynamic CT imaging tracks closely and correlates with physical measurements of tissue stiffness as determined by the Young's moduli of the extracted nodules.

Methods and Materials

Cell Culture

A549 human lung carcinoma cells were obtained from ATTC (CCL-185) and cultured in F-12K medium supplemented with 10% FBS and 1% penicillin-streptomycin and incubated in 95% air/5% CO_2 at 37°C.

Animal Models and Pulmonary Nodule Generation

All experiments were conducted following approval by the Administrative Panel on Laboratory Animal Care (APLAC) of Stanford University. A total of 15 RNU female rats (Taconic Biosciences, Petersburgh, NY) were anesthetized using 2% isoflurane and placed inside the Spectral Ami X Optical imaging instrument (Tucson, Arizona). The scanner used to facilitate high-precision image guidance for injection and localization within the lung. In each case, a 1 cc syringe with a 30G needle was introduced through the intercostal space and held in place inside the lung of the anesthetized rat. Before injection, an X-ray image was obtained to determine whether the needle was placed within the desired location (Figure 1). Three different types of PNs were generated in the animals: (i) Talc-20 mg of talc/80 μl PBS (Sigma-Aldrich, St. Louis, MO) was injected into each right lung. (ii) Tumors - to generate orthotopic lung tumor models, 7 rats, some of which had been previously injected with talc in the right lung, underwent whole body irradiation (4 Gy). A total of 2×10^6 A549 lung cancer cells in matrigel (diluted 1:1 in PBS) in a final volume of 80 μl were then injected into the intercostal space of the left lung 24 hours after irradiation. The rats were then monitored for 60 min to ensure they showed no negative side effects from the procedure. (iii) Matrigel - To simulate NPNs with different mechanical properties from malignant A549 lung tumors, matrigel (80 μl) was injected into the right lung of another 7 rats, all of which had been previously injected with talc in the left lung. Injection of each compound. Implantation of each substance was completed only after X-ray images confirmed the needle had been placed in the right location within the lung.

Respiratory-Gated MicroCT Imaging

The timelines from injection into the lung to MicroCT imaging differed for each PN and were as follows: Talc – Imaged 5 days to 8 weeks post injection; A549 lung cancer cells – Imaged 4 to 5 weeks post inoculation; Matrigel – Imaged 60 to 90 min post injection. The rats were anesthetized and maintained under 2% isoflurane in oxygen. Scanning was performed with an eXplore Locus RS-150 MicroCT rodent model instrument (GE Healthcare., Fairfield, CT) fitted with a nose cone for isoflurane anesthesia administration [17]. X-rays were generated from a 70-kVp, 40-mAmp source with the following acquisition parameters: 400 views over an angle of increment of 0.9°, averaging 2 frames per view; exposure time: 17ms; resolution: 0.095943mm; with 4 × 4 binning on the charge coupled device detector.

MicroCT Image Reconstruction

Image reconstruction was performed using eXplore MicroView. Each scanned image was centered in a 46.25-mm axial field of view (84.7 mm transaxial field of view). Images were first calibrated and corrected, and reconstruction was performed at an isotropic resolution of 97.3 μm. Extreme tidal volume images, obtained at peak inhale and exhale, were acquired with a temporal resolution of 15 ms by respiratory gating using the Biovet software program.

Image Analysis and Derivation of a Volumetric Change Parameter (δ)

Post-acquisition analysis for the 2 respiratory phases was performed by 4 observers using the treatment planning software, Eclipse V11 (Varian Medical Systems, Inc., Palo Alto, CA, USA). To compensate for inter-observer variability, the average volume of the PNs delineated by the 4 observers was used in determining the volumetric change of each nodule. Nodule delineation and volume changes were determined through contouring: regions of interest (ROIs) were drawn on every slice to delineate each nodule and subsequently merged to form 3-dimensional volumes for each tidal extreme (inhale or exhale). A deformability parameter (δ) was defined as the ratio of the volumetric change of the PN between inhale and exhale (**Equation 1**). Zero implied no volumetric changes as would be expected for stiffer nodules. Values significantly different from zero implied less stiff nodules, as these nodules would either expand or contract significantly going from one respiratory cycle to the next.

Briefly,

$$\delta = \frac{V_{inhale}}{V_{exhale}} \qquad (1)$$

where V represents the volume obtained from image analysis.

Histology

Hematoxylin and eosin stain (H&E staining) was performed for 3 rats with each nodule type immediately following MicroCT imaging. Briefly, the animals were euthanized with carbon dioxide and the lungs harvested and placed in 4% paraformaldehyde for 24 hours. They were subsequently enclosed in a cassette and stored in 100% ethanol until they were embedded in paraffin and sectioned. Images were obtained using a flurorescent microscope.

Atomic Force Microscopy

Atomic force microscopy (AFM) was used to measure tissue stiffness. Force-distance (FD) measurements of excised tissues were done in a fluid cell. Measurements were taken either using an Agilent 5500 Scanning Probe Microscope (Agilent Technologies, Santa Clara, CA) or a Park NX-10 AFM (Park Systems, Santa Clara, CA) when temperature control was necessary. The moduli were verified and reproduced on both machines for all samples with the exception of the matrigel samples, which could only be analyzed using the NX-10 at 37^{o}C in order to remain a solid gel. Samples were probed a minimum of 10 times in at least 3 distinct regions 20 μm apart for obtaining a representative result. Young's moduli were calculated using the Hertz theory for spherical indenters from the shape of the initial indentation curve.

Statistical analysis

Statistical analysis was performed using SAS 9.4 software (SAS Institute Inc., Cary NC). Pearson's correlation coefficient was determined to establish whether there was a significant degree of linear dependence between the non-invasive nodule volume changes from respiratory-gated dynamic CT and their physical stiffness as determined by AFM measurement.

Results

High-precision image guidance for injection and localization using the Spectral Ami X Optical imaging (**Figure 1**) ensured successful PN establishment in the left (matrigel or A549 tumor) and right (talc) lungs (**Figure 2**). PNs formed from talc were particularly heterogeneous with some calcified nodules identifiable on MicroCT imaging. MicroCT gating (**Supplementary 1**) ensured the acquisition of CT images only at extreme tidal volumes (**Supplementary 2**). An overlay of the images acquired at peak tidal volumes (**Figure 3**) indicated that the inflated lung volume, on average, was 16% higher than the non-inflated lung. Percentage increases of

4, 1 and less than 1% were observed for nodules from matrigel, tumor, and talc, respectively from exhale to peak inhale. The mean volumes at peak inhale for the tumor, matrigel, talc, and lung were 0.04, 0.21, 0.03, and 3.91, respectively. Corresponding values for exhale, respectively, were 0.04, 0.20, 0.03 and 3.20. The volumetric ratio, exhale to inhale for matrigel, tumor, and talc were 1.05, 0.96 and 1.01, respectively. The corresponding lung volumetric ratios for each nodule were 0.82, 0.90, and 0.89 for lungs with matrigel, tumor, and talc, respectively.

To validate our non-invasive method, AFM was used to determine the stiffness of PNs. FD measurements (**Figure 5A**) were taken to determine the Young's moduli, and our sample positioning and representative test regions are shown in **Figure 5B**. The range of elastic moduli for tumor, talc, and matrigel PNs is shown in **Figure 5C**. The average Young's modulus for the tumor was significantly higher than those for matrigel and the normal lung tissue (data not shown) but was not significantly different from talc. The mean value for the tumors was 2552 Pa, in comparison to values of 1287 Pa and 1304 Pa for matrigel and lung tissue, respectively. Tumor stiffness was thus 98% and 96% higher than for matrigel and normal lung tissue, respectively. There were no significant differences in stiffness between matrigel and talc. H&E staining showed the localization of the tumors and matrigel inside the lungs in comparison to lungs from control rats (**Figure 6**). There was a significant correlation between the nodule volume changes determined by the non-invasive methodology and physical measurements of stiffness **(Figure 7).**

Discussion

In the present study, we sought to evaluate a non-invasive imaging methodology in a rat model of orthotopic human lung cancer and non-malignant lesions by comparing the nodule volumetric changes on CT imaging to physical measurements of nodule stiffness. We further sought to determine whether we could non-invasively differentiate between pulmonary nodules that appeared similar on CT images but had different tissue characteristics based their deformability at extreme tidal volumes.

The present study demonstrated that our non-invasive imaging methodology correlated very strongly with the physical measurements of stiffness obtained from AFM. AFM FD allows for probing tissue elasticity on a local scale compared to macroscopic rheology and at much higher strain rates. We demonstrated that tissue stiffness is directly related to nodule volumetric changes obtained from non-invasive respiratory-gated CT

imaging. We further demonstrated the robust performance and sensitivity of the imaging methodology by showing that minute changes in nodule volume could be measured and analyzed to determine changes in tissue characteristics between different nodules.

Screening for tumors by determining tissue stiffness has been used in a number of studies to predict tumor malignancy. Colorectal liver metastasis and normal liver are reported to have mean interstitial pressure of 21 and 7 mmHg, while breast carcinomas have mean interstitial pressure of 15 mmHg versus normal breast pressure of 0 mmHg [Ref]. In the present study, the animal models were based on the differences in stiffness for malignant versus non-malignant tissues. To validate the imaging methodology, an orthotopic lung tumor model using A549 cells in rats was created (Ref). These cells were malignant, and the resulting tumors were expected to be stiffer than the surrounding normal lung tissue. To create a non-malignant model, matrigel, which is a solubilized basement membrane preparation extracted from mouse sarcoma and enriched with a number of growth factors was injected into the rat lung. At 37 ^{o}C, matrigel forms a gel within the lung, which appears as a nodule upon CT imaging, indistinguishable from a malignant nodule (**Figure 2**). We hypothesized that the properties of matrigel differ significantly from the tumor nodules such that its stiffness would be substantially less than that of tumor. Our third animal model involved the use of talc in forming the pulmonary nodules. Unlike matrigel or A549 lung cancer cells which resulted in consistent nodules of similar tissue characteristics, nodules from talc ranged from deposits of hard crystal aggregates to softer gel-like granulomas. We thus anticipated that their volumetric changes and Young's moduli (as a measurement for stiffness) would exhibit greater variation than those for tumor or matrigel nodules.

In a previous publication, we defined an expression for the term, elasticity (d_e) for pulmonary nodules as

$$d_e = \frac{|\varphi_{DIR,MPN}-1|}{|\varphi_{DIR,ring}-1|} \quad (3),$$

where $\varphi_{DIR,MPN}$ and $\varphi_{DIR,ring}$ are the volumetric ratios of the pulmonary nodule and lung, respectively [REF]. However, in the same study, we acknowledged that there were many possible expressions for the definition of elasticity, all of which were only surrogates for a physical measurement that required knowledge of applied forces that cannot be determined from non-invasive imaging. The present study focused on changes in pulmonary nodule volume and morphology going from one extreme tidal volume to the other as detected by non-invasive and compared the changes to physical measurements. The study successfully demonstrated that

the volumetric changes of PNs with different tissue characteristics as determined by dynamic respiratory-gated MicroCT imaging was similar to physical measurements of nodule stiffness obtained from application of an an external force indicating that malignant and non-malignant PN differed in tissue characteristics. The differences may be attributed to increased interstitial fluid pressure as reported for breast carcinoma [2,3], metastatic melanoma [4,5], head and neck carcinoma [6], and colorectal carcinoma [2]. The interstitial fluid pressure may change the tissue characteristics of the PN and other minute morphological features which then form the basis for the ability of our non-invasive methodology to distinguish between the different pulmonary nodules. While the mechanisms underlying the increased tumor interstitial fluid pressure have not been fully elucidated, it has been shown that the pressure is uniform throughout the center of the nodule but drops steeply towards the periphery.[21-23]. The mechanisms are thought to involve blood-vessel leakiness, lymphatic vessel abnormalities, interstitial fibrosis and a contraction of the interstitial space mediated by stromal fibroblasts, all of which are hallmarks of cancer [24,25].

A limitation of current CT based screening for lung cancer is the inability to effectively distinguish malignant from non-malignant nodules [26]. This non-invasive methodology could have an impact on clinical practice by increasing the specificity of CT-based lung cancer screening. PNs that undergo very little volumetric changes from one extreme tidal volume to the next may also serve as predictors of tumor aggressiveness and could potentially be used in multifocal lung cancer patients to identify and treat the most aggressive lesions first. Ultimately, the methodology may also serve as a guide to radiation therapy dose painting or adaptive boost design by identifying the aggressiveness of different tumor regions.

The primary limitation of this study involved generating the non-malignant nodules. Clinically, benign nodules are a heterogeneous group of neoplastic lesions. These include hamartoma, lipoid granuloma, lipoma, lung cysts and intrapulmonary lymph nodes. Several autoimmune diseases, infections and vascular abnormalities such as malformations of the blood vessels in the lungs including hemangioma, cavernous angioma and pulmonary telangiectasis can also lead to pulmonary nodule development. We were unable to create animal models covering all the various forms and sources of non-malignant nodules. While we cannot claim that our methodology distinguishes every kind of non-malignant nodule from a malignant one, we have demonstrated that the non-invasive results tracks very closely with physical measurements of nodule stiffness. It could

potentially be used as a routine highly sensitive and specific screening tool in a prospective clinical trial to detect the early onset of lung cancer ultimately resulting in a reduction in mortality.

Conclusion

We successfully demonstrated that a preclinical, noninvasive image-processing methodology based on inhale/exhale breath-hold images could detect PN volumetric changes and these changes correlated with physical measurements of nodule stiffness.

Figures

Figure 1: Representative spectral AMI X image-guided implantation of cells, talc and matrigel to form pulmonary nodules

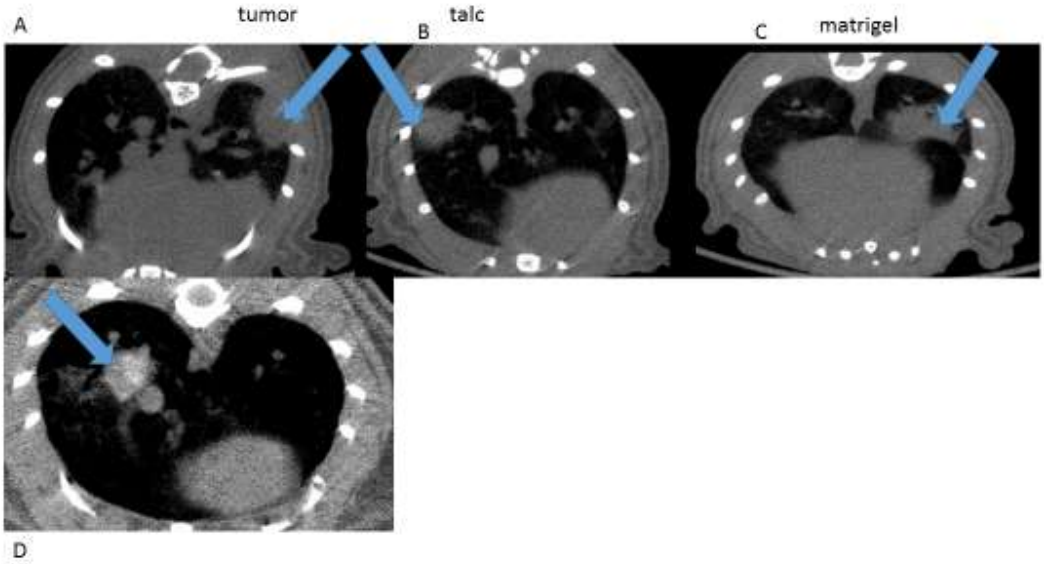

Figure 2: Representative MicroCT images of the rat lung obtained at peak inhale showing pulmonary nodules formed from malignant A549 carcinoma cells (A), talc (B) and matrigel (C); In some animals, nodules from talc became calcified over time (D). The arrows denote each nodule

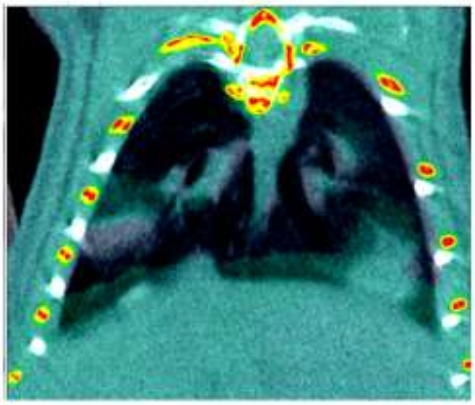

Figure 3: An overlay of respiratory-gated MicroCT images of the thoracic region of the rat at peak inhale (black and grey) and peak exhale (rainbow)

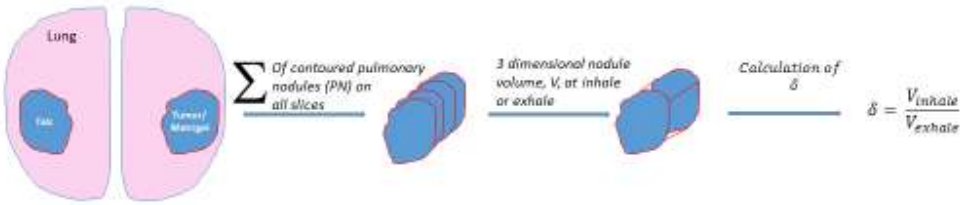

Figure 4: Schematic diagram showing the derivation of volumetric changes from pulmonary nodules. Values were generated by contouring regions of interest (ROIs) drawn on every Micro CT image slice to delineate each nodule and subsequently added up to form a 3-dimensional volume representing the whole nodule.

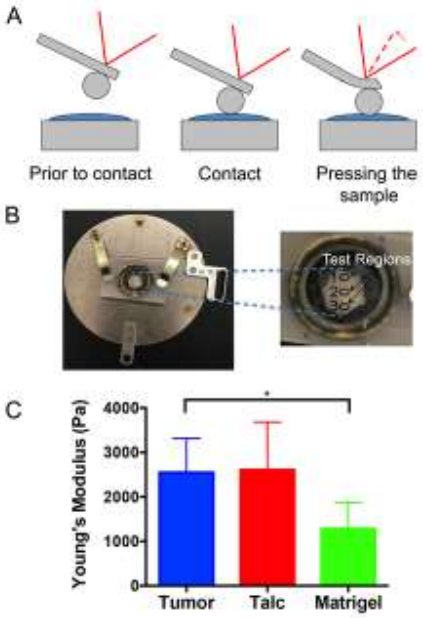

Figure 5. Measuring the elasticity of biological tissues using AFM. **(A)** Schematic of AFM using a spherical tip for FD measurements. **(B)** Lung tumors in the AFM sample holder and sites of modulus measurements. Samples were probed 10 times in each region for accurate measurements. **(C)** Young's moduli of rat lung tumor, matrigel, and lung tissue samples using the Hertz model. Error bars show standard deviation.

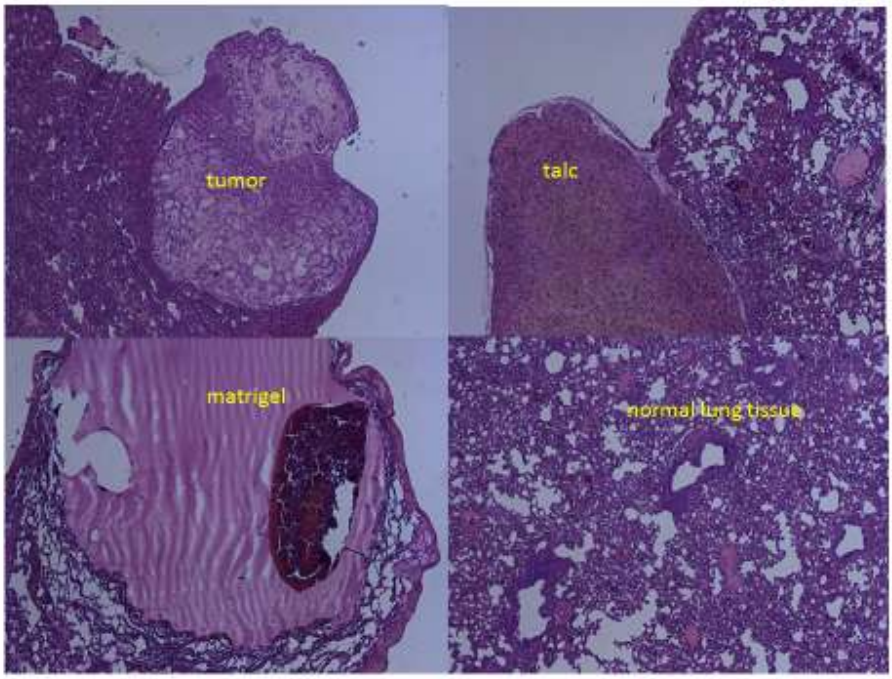

Figure 6: Hematoxylin and eosin stain (H&E staining) for pulmonary nodules derived from A549 cells, talc and matrigel compared to normal lung tissue

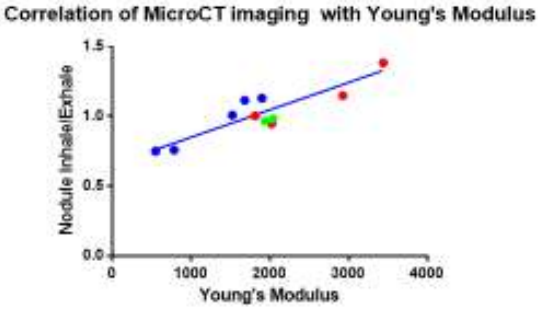

Pearson r	
r	0.8957
95% confidence interval	0.6394 to 0.9728
R squared	0.8023
P value	
P (two-tailed)	0.0002
P value summary	***
Significant? (alpha = 0.05)	Yes
Number of XY Pairs	11

Figure 7: Correlation of volumetric changes with tissue stiffness

Supplementary Figure 1: A representative anesthetized female NIHRNU rat (Taconic) placed on a MicroCT scanner with a probe for respiratory-gated imaging

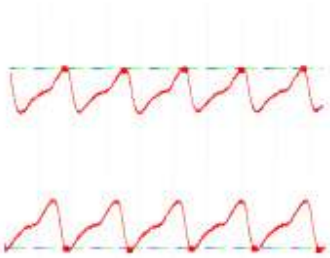

A

B

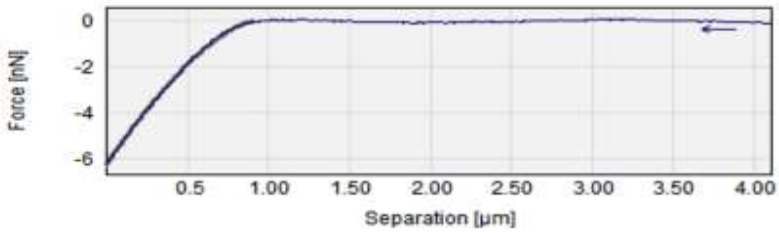

Supplemental. A) FD curve example. B) Fit example

References

1. Mountain CF. Revisions in the International System for Staging Lung Cancer. *Chest*. 1997: 111:1710-1717.
2. Aberle DR, Berg CD, Black WC, Church TR, Fagerstrom RM, Galen B et al. The National Lung Screening Trial: overview and study design. *Radiology*. 2011: 258:243-253.
3. Negandar M, Fasola CE, Yu AS, von Eyben R, Yamamoto T, Diehn M et al. Noninvasive pulmonary nodule elastometry by CT and deformable image registration. *Radiother Oncol*. 2015: 115:35-40.
4. Kabus S, Klinder T, Murphy K, van Ginneken B, van Lorenz C, Pluim JP. Evaluation of 4D-CT lung registration. *Med Image Comput Comput Assist Interv*. 2009: 12:747-754.
5. Kabus S, Franz A, Fischer B. Spatially varying elasticity in image registration. *Methods Inf Med*. 2007: 46:287-291.
6. Guerrero T, Zhang G, Huang TC, Lin KP. Intrathoracic tumour motion estimation from CT imaging using the 3D optical flow method. *Phys Med Biol*. 2004: 49:4147-4161.
7. Nonomura K, Shimamoto K, Hatasa K, Mizuno M, Machida K, Mizuno H et al. Differential diagnosis of breast mass image-forming lesions based on changes in depth-width ratio and internal echo intensity by hand-held probe compression. *Journal of Medical Ultrasonics*. 2008: 35:63-69.

Appendices:

Accepted manuscript in Radiotherapy and Oncology:

“**Noninvasive pulmonary nodule elastometry by CT and deformable image registration**”

Radiotherapy and Oncology 115 (2015) 35–40

Contents lists available at ScienceDirect

Radiotherapy and Oncology

journal homepage: www.thegreenjournal.com

Thymoma

Noninvasive pulmonary nodule elastometry by CT and deformable image registration

Mohammadreza Negahdar [a], Carolina E. Fasola [a], Amy S. Yu [a], Rie von Eyben [a], Tokihiro Yamamoto [d], Maximilian Diehn [a], Dominik Fleischmann [b], Lu Tian [c], Billy W. Loo [a,*], Peter G. Maxim [a,*]

[a] Department of Radiation Oncology; [b] Department of Radiology; [c] Department of Health Research and Policy, Stanford University; and [d] Department of Radiation Oncology, University of California, Davis, United States

ARTICLE INFO

Article history:
Received 16 August 2014
Received in revised form 6 March 2015
Accepted 15 March 2015
Available online 27 March 2015

Keywords:
Malignant pulmonary nodule (MPN)
Elasticity
Deformable image registration (DIR)
X-ray CT
Lung cancer

ABSTRACT

Background and purpose: To develop a noninvasive method for determining malignant pulmonary nodule (MPN) elasticity, and compare it against expert dual-observer manual contouring.
Methods and materials: We analyzed breath-hold images at extreme tidal volumes of 23 patients with 30 MPN treated with stereotactic ablative radiotherapy. Deformable image registration (DIR) was applied to the breath-hold images to determine the volumes of the MPNs and a ring of surrounding lung tissue (ring) in each state. MPNs were also manually delineated on deep inhale and exhale images by two observers. Volumes were compared between observers and DIR by Dice similarity. Elasticity was defined as the absolute value of the volume ratio of the MPN minus one normalized to that of the ring.
Results: For all 30 tumors the Dice coefficient was 0.79 ± 0.07 and 0.79 ± 0.06 between DIR with observers 1 and 2, respectively, close to the inter-observer Dice value, 0.81 ± 0.1. The elasticity of MPNs was 1.24 ± 0.26, demonstrating that volume change of the MPN was less than that of the surrounding lung.
Conclusion: We developed a noninvasive CT elastometry method based on DIR that measures the elasticity of biopsy-proven MPN. Our future direction would be to develop this method to distinguish malignant from benign nodules.
 Radiotherapy and Oncology 115 (2015) 35–40

Elastometry provides tissue characterization that may help distinguish malignant from benign tissues, in contrast to static morphological imaging, which cannot provide this degree of information [1]. Several modalities of elasticity imaging, mostly based on ultrasound have been proposed and applied to a number of clinical applications including breast carcinoma [2,3], metastatic melanoma [4,5], head and neck carcinoma [6], and colorectal carcinoma [2]. However, since air is opaque in ultrasound images, this imaging modality has been considered insufficient for adequately visualizing lung tissue. Magnetic resonance elastography is an MRI-based technique which is capable of assessing tissue stiffness and is beneficial for example to assess hepatic fibrosis [7,8]. However this method similarly suffers from susceptibility artifacts from air in the lung.

Dynamic CT (including cine-CT and four dimensional (4D) CT) images the lung in different states of expansion that could be used to derive elasticity information in contrast to static three dimensional (3D) CT. In this study, we propose to develop pulmonary nodule elastometry derived from CT images acquired at breath-hold at extreme tidal volumes. We applied deformable image registration (DIR) to the breath-hold images to determine the volume of the malignant pulmonary nodules (MPN) and a ring of the surrounding lung tissue in each respiratory state. Then, elasticity was defined as the ratio of the volume change of MPN compared to the ring.

To demonstrate proof of principle that pulmonary nodule elastometry can be determined from breath-hold CT images at extreme tidal volumes, we analyzed the pre-treatment CT images of 23 patients with malignant pulmonary nodules (MPN) treated with stereotactic ablative radiotherapy (SABR) at our institution and compared the volume change of the treated MPN with that of the surrounding lung.

Methods and materials

Patient selection

From all patients treated on an institutional protocol of stereotactic ablative radiotherapy (SABR) for lung tumors between

* Corresponding authors at: Stanford Cancer Center, 875 Blake Wilbur Dr., Stanford, CA 94305, United States.
E-mail addresses: bwloo@stanford.edu (B.W. Loo), pmaxim@stanford.edu (P.G. Maxim).

http://dx.doi.org/10.1016/j.radonc.2015.03.015
0167-8140/

November 2011 and October 2012, 23 patients had both inhale and exhale breath-hold CT scans performed at the time of simulation available for review and are included in this analysis.

CT imaging

Deep inspiration and natural expiration breath-hold CT scans for these patients were acquired on a Discovery ST PET/CT Scanner (General Electric Medical Systems, Waukesha, WI, USA), using the following acquisition settings: 120 KVp, 110–195 mAs, 1.25 mm slice thickness, 0.97–1.36 mm pixel size, 500–700 mm display field of view. Images were reconstructed using either the built-in Bone Plus or Soft convolution kernel.

Contouring

The original treatment plans were delineated on either exhale or deep inhale based on the treating physician's clinical judgment regarding which to use for treatment, and the clinically used contours were taken as reference. Two observers manually delineated the MPN on the opposite respiratory phase using our treatment planning software, Eclipse V11 (Varian Medical Systems, Inc., Palo Alto, CA, USA). For manual delineation, each observer applied the standard pre-defined "Lung" window-level (window width: 1324 HU, window level: −362 HU) when contouring the tumors. To address inter-observer variability, the MPNs delineated by the two observers were compared to each other by calculating the Dice similarity coefficient voxel-wise [9,10].

Deformable image registration

An intensity-based free-form deformable image registration (DIR) workflow was developed in MIM Maestro (MIM Software Inc., OH, USA) and applied on extreme tidal volumes to determine the deformation map between deep inhale and natural exhale images. The underlying algorithm parameters were inherent in the program. The similarity and smoothness criteria were combined into one energy function, which was minimized in the registration process [11]. Since the main effect of respiration on MPN is the transition of MPN whereas deformation and volume change of MPN is minimal [12], we separate effect of large displacement between two extreme breath-hold images from volume changes of MPN itself. Therefore the workflow starts with a tumor to tumor rigid registration with manual adjustment, followed by the DIR method which deforms the inhale (source) image to exhale (target). Rigid registration and manual adjustment yield the advantage of robustness to the MPN location.

DIR validation

We adopted the Dice similarity coefficient to assess the quality of overlap between the manually delineated contours and deformed contours [13]. As shown in Fig. S1 (a) (Supplementary data), for patients with MPNs originally delineated on inhale, DIR was used to create an exhale contour. The deformed contours were then compared to the two manually delineated exhale contours using the Dice similarity metric. Similarly and as shown in Fig. S1 (b) (Supplementary data), for patients with MPNs originally delineated on exhale, the two observers manually delineated contours on deep inhale. Next, DIR was used to create exhale contours from the manually delineated contours on deep inhale. These deformed contours were then compared to the clinically delineated contour by Dice.

Quantitative analysis of the deformation map

Because of the need for one-to-one correspondence between material points during continuous deformation, the calculated Jacobian determinant is required to be non-zero [14,15]. The degree of regional lung expansion is measured using the Jacobian determinant of the deformation map which is directly related to specific volume change [14].

$$J_n = \frac{V_n + \Delta V_n}{V_n} \tag{1}$$

where V_n is the volume of voxel element n, and ΔV_n is its change in a different respiratory cycle. A value of one implies no volumetric changes, while a Jacobian determinant greater than one, or smaller than one implies local tissue expansion or local tissue contraction, respectively. It therefore follows that for a continuous deformation to be physically possible, the Jacobian determinant must be greater than zero. We took advantage of this fact to evaluate the accuracy of the calculated deformation map.

To validate the volumetric changes as determined by the DIR method, we used the manually delineated MPNs. The volumetric changes were expressed as the ratio of the volumes in both phases.

$$\varphi_{manual} = \frac{V_{exhale}^{MPN}}{V_{inhale}^{MPN}} \tag{2}$$

where φ_{manual} is the manually measured volume ratio of MPN, V_{inhale}^{MPN} is the volume of the MPN at deep inhale and V_{exhale}^{MPN} is the volume of the MPN at natural exhale.

Elasticity

We derived an elasticity parameter defined as the ratio of the volumetric change of the MPN to the volumetric change of a 1 cm ring of lung tissue surrounding the MPN, Fig. 1:

$$d_\varepsilon = \frac{|\varphi_{DIR_{MPN}} - 1|}{|\varphi_{DIR_{Ring}} - 1|} \tag{3}$$

Where $\varphi_{DIR_{MPN}}$ is the calculated volumetric ratio (exhale/inhale) of MPN and $\varphi_{DIR_{Ring}}$ is the calculated volumetric ratio (exhale/inhale) of a 1 cm ring around the MPN. As stated above, in some cases the clinically delineated volume was on the exhale CT and in some it was on the inhale CT, but in all cases the volume ratios (φ_{DIR}) were taken to be the exhale to inhale ratio. The normalization to the 1 cm ring around the MPN, was introduced to remove the effect of MPN location and amount of motion in the lung, as both the MPN and the 1 cm ring surrounding lung tissue undergo the same force. The choice of using a 1 cm ring surrounding the MPN's is somewhat arbitrary, however based on the size of the tumors, this ring size allows equal contribution of lung tissue and MPN into the calculated elasticity parameter. The calculated elasticity bigger than one ($d_\varepsilon > 1$) shows that the volume changes of MPN is more than that of the ring and the calculated elasticity smaller than one ($d_\varepsilon > 1$) shows that the volume changes of MPN is less than that of the ring.

Statistical analysis

An equivalence test was performed to assess that the manually measured volume ratio was equivalent to the DIR calculated volume ratio of MPN. A paired t test was performed to compare the volume change of the normal tissue and the tumor tissue with both tissue samples coming from the same patient. All analyses were performed using SAS version 9.4 (SAS Institute Inc., Cary, NC, USA).

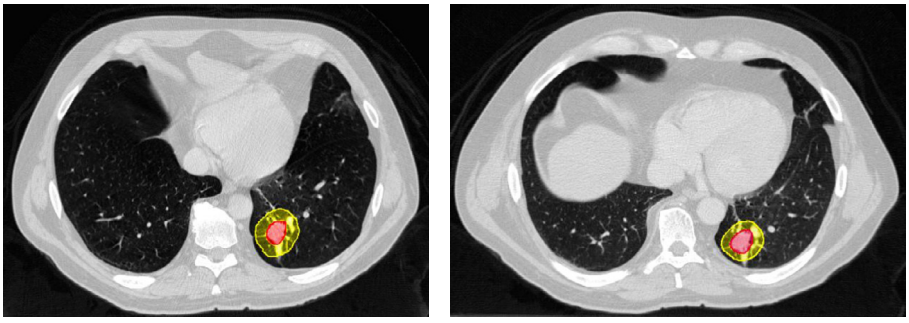

Deep Inhale CT **Natural Exhale CT with Deformed Contours**

Fig. 1. An axial view of a representative patient; delineated MPN (inner circle) and 1 cm ring of the surrounding lung (outer circle) for deep inhale (left column) and deformed MPN and ring contours superimposed on exhale image (right column) for the purpose of elasticity calculation.

Results

Patient and tumor characteristics

We have included 23 lung cancer patients with primary non-small cell lung cancer (NSCLC) or limited lung metastases that were treated at our institution. The patient and tumor characteristics are given in Table 1.

DIR validation

For all patients, the Dice similarity coefficient between the delineated tumors by observer 1 and that of observer 2 is 0.81 ± 0.1, whereas the Dice value is 0.79 ± 0.07 and 0.79 ± 0.06 between DIR and observer 1 and DIR and observer 2, respectively. Fig. 2 shows an example of both delineated and deformed contours for a representative patient as well as the distribution of the calculated Dice similarity for all patients. For all patients we calculated the Jacobian determinant of the deformation map and validated the calculated volume ratio of MPN from the deep inhale phase to the natural exhale phase against the manual contouring. The calculated Jacobian determinant of the deformation map within the lung is always greater than zero. We performed an equivalence test with the indifference zone defined as [−0.25, 0.25]. The mean of the differences of the paired values was 0.0293 with a 95% confidence interval of [−0.0176, 0.0761]. The 95% confidence interval falls completely within the indifference zone thus proving equivalence ($p < 0.0001$). The average difference between the manually measured volume ratio of MPN (φ_{manual}) and calculated volume ratio value via DIR ($\varphi_{DIR_{MPN}}$) was 0.02 ± 0.15. Fig. 3 shows the calculated volume ratio by DIR versus manually measured volume ratio of MPN for all patients as well as the distribution of the difference between the calculated volume ratio and manually measured volume ratio of MPN for all patients which mainly concentrated around zero.

Table 1
Patient and tumor characteristics.

Characteristic	Value (%)
All Patients	23
Gender	
Male	13 (57)
Female	10 (43)
Age, *y*	
Median	66
Range	35–94
Tumors	30
Primary/secondary	18/12
Histology	
Adenocarcinoma	21
Squamous	9
Radius of tumors, cm (treatment planning)	
Median	1
Range	0.3–2.1
Volume of tumors, cm^3 (treatment planning)	
Median	4.21
Range	0.11–38.8
Volume of tumors in opposite phases, cm^3 (Obs 1)	
Median	4.3
Range	0.13–39.62
Volume of tumors in opposite phases, cm^3 (Obs 2)	
Median	4.29
Range	0.13–39.74

MPN elasticity

For all patients in our study, the mean and standard deviation of the calculated volume ratio of the MPN and that of the 1 cm ring surrounding lung tissue was 0.91 ± 0.18 and 0.75 ± 0.13, respectively. The mean and standard deviation of the difference between the calculated volume ratio of the MPN ($\varphi_{DIR_{MPN}}$) with that of 1 cm ring surrounding lung tissue ($\varphi_{DIR_{Ring}}$) was 0.16 ± 0.15 ($p < 0.0001$). Fig. 4(a) shows the calculated volume ratio of MPN and 1 cm ring surrounding lung tissue for all patients. The volume ratio is mainly distributed below the unity line demonstrating that the volume ratio of the MPNs is less than that of the 1 cm ring surrounding lung tissue.

Finally, based on our definition of the elasticity parameter in Eq. (3), the mean and standard deviation of the calculated elasticity (d_e) of the MPN was 0.78 ± 1.1, and the median value was 0.58. Fig. 4(b) shows the distribution of the calculated elasticity for all patients.

Table 2 (Supplementary data) shows tumor size in inhale and exhale, as well as the calculated volume ratio of MPN by DIR, the calculated elasticity, histology, and lobar location. The median elasticities for lower and upper/middle lobe MPNs are 0.53 and 0.61, respectively.

Discussion

We have designed and developed a method to determine the elasticity of MPNs based on deformable image registration of breath-hold CT images. Various deformable image registration methods [12,16–19] and mechanical indices [20] have been surveyed to calculate the most accurate and robust deformation map as well as differentiation metric, respectively. We developed a workflow that processed breath-hold images at extreme tidal volumes and calculated the volume change and the elasticity of MPNs.

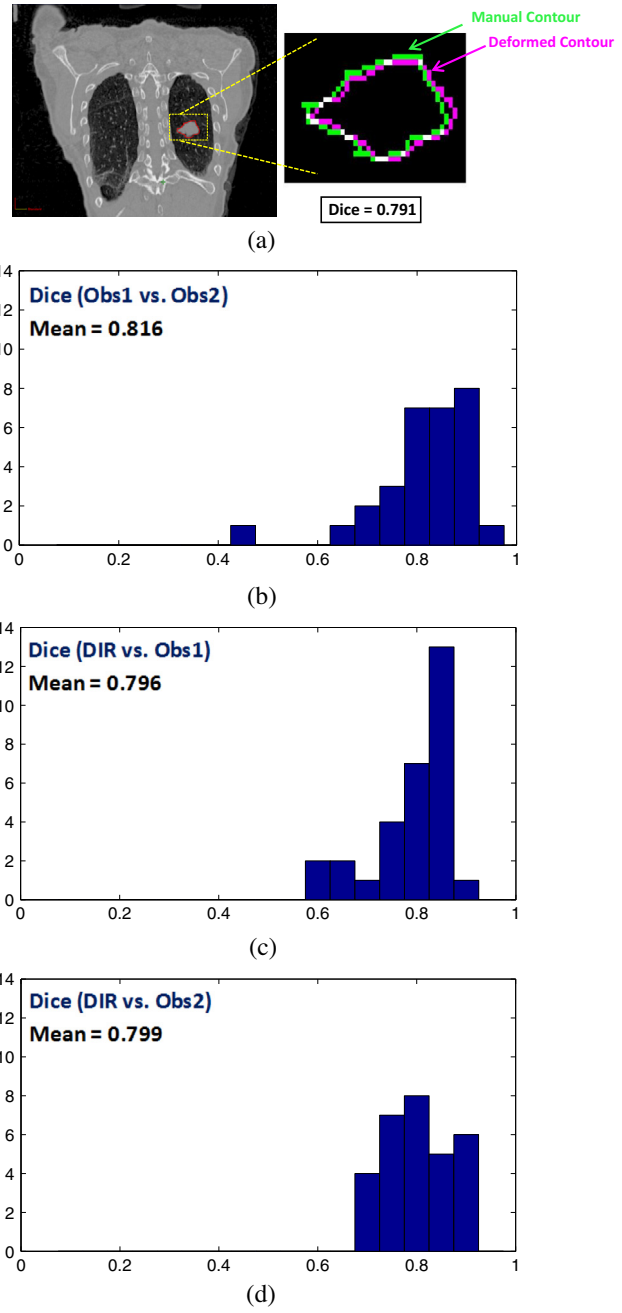

Fig. 2. (a) A coronal view of a manually delineated tumor in exhale of a representative patient; delineated MPN in exhale (green) and delineated MPN in inhale deformed into the exhale (magenta), Dice similarity for this patient is 0.791. (b) Distribution of the calculated Dice similarity metric between the manually delineated MPN by first observer with that of second observer. (c) Distribution of Dice similarity between the delineated MPN in inhale deformed into the exhale phase by DIR with the manually delineated MPN by first observer in exhale. (d) Distribution of Dice similarity between the delineated MPN in inhale deformed into the exhale phase by DIR with the manually delineated MPN by second observer in exhale. Based on dice similarity, we conclude that DIR compares favorably to manual contouring within inter-observer differences. (For interpretation of the references to colour in this figure legend, the reader is referred to the web version of this article.)

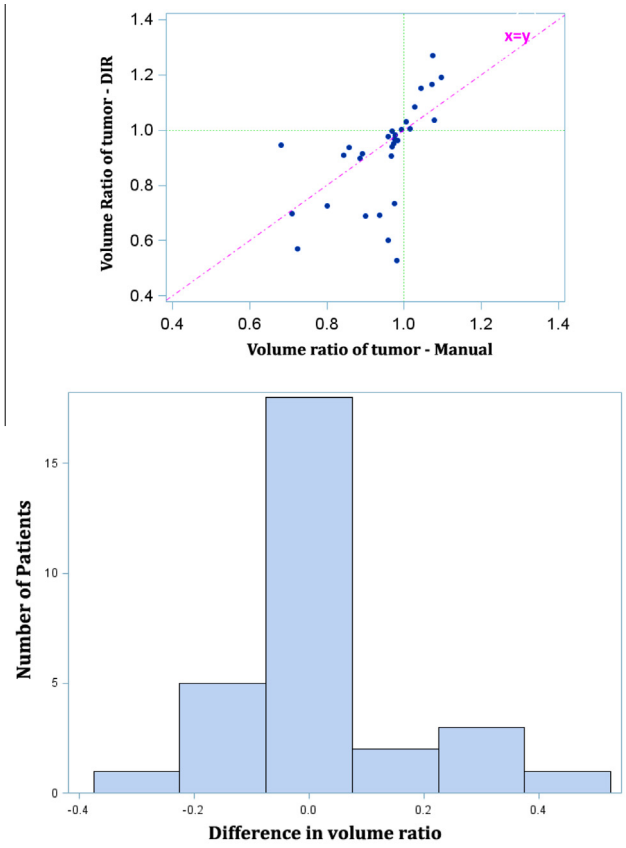

Fig. 3. (Up) Calculated volume ratio of MPN versus manually measure of volume ratio of MPN (Eq. (2)) for all 30 patients from inhale to exhale. Green dashed line shows unity Jacobian value equivalent to no volume changes. Red line represents the identity line (Bottom). Distribution of the difference between the calculated volume ratio by DIR from inhale to exhale with manually measured volume ratio of MPN (0.02 ± 0.15). (For interpretation of the references to colour in this figure legend, the reader is referred to the web version of this article.)

We have demonstrated robust performance of the DIR method such that the difference between DIR and each of the observers is comparable to the inter-observer difference as assessed by Dice similarity. Our method can measure the volume ratio of MPNs, which can be either expansion or contraction. The accuracy of this measurement is demonstrated by the small difference between the manually measured volume ratios to that of the DIR method (0.02 ± 0.15).

Based on the presented results in Fig. 4(a), $0 < \varphi_{DIR_{Ring}} < \varphi_{DIR_{MPN}} < 1$ which demonstrates that MPNs have a lesser volume change than the 1 cm ring surrounding lung tissue during exhalation. Thus, one expects $d_\varepsilon = \frac{|\varphi_{DIR_{MPN}} - 1|}{|\varphi_{DIR_{Ring}} - 1|} < 1$ which has been shown in Fig. 4(b), ($d_\varepsilon = 0.78 \pm 1.1$). This demonstrated that MPNs have different characteristics in terms of elasticity compared to the surrounding lung tissue during respiration.

Different parts of the lung have different motion amplitudes and volume changes, which makes the calculated volume ratio of MPNs location-dependent. However the formulated elasticity is not location-dependent because the normalization of the volume change of MPN to that of the 1 cm ring surrounding lung tissue should remove the effect of MPN location, as both the MPN and the 1 cm ring surrounding lung tissue undergo the same force, irrespective of their location. Therefore, it allows us to compare the elasticity of two different MPNs in two different locations of lung. This is supported by the similar median values of the elasticity parameter for lower vs. upper/middle lobe MPNs.

Our study does have certain limitations. First, our method was applied to a small number of patients, and focused only on proven MPNs, excluding benign nodules. The imaging protocol for all patients was not completely uniform which resulted in different image resolutions that can impact the analysis. However we

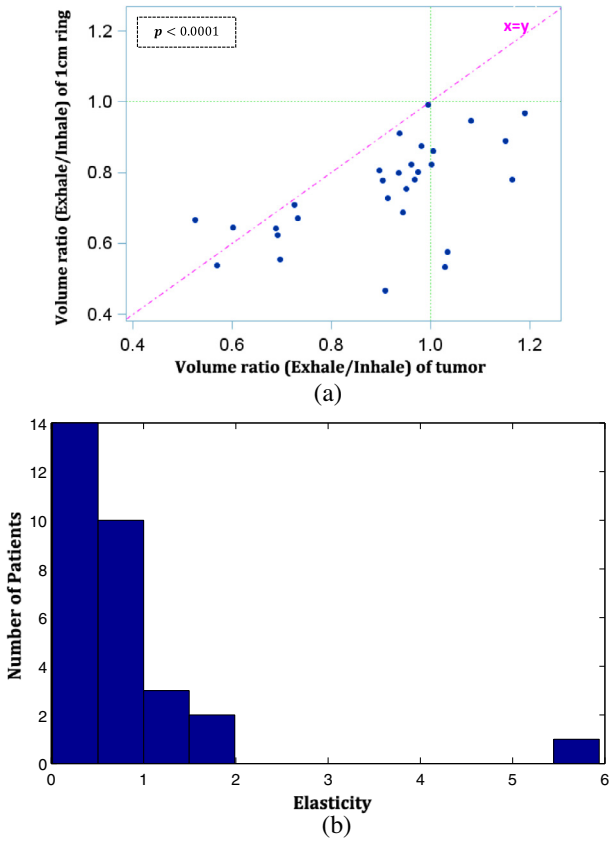

Fig. 4. (a) Calculated volume ratio of 1 cm ring of surrounding lung (0.75 ± 0.13) versus that of tumor (0.91 ± 0.18) for all patients. Green dashed line shows unity Jacobian value equivalent to no volume changes. Red line represents the identity line. (b) Distribution of the calculated elasticity by Eq. (3) from inhale to exhale (0.78 ± 1.1). (For interpretation of the references to colour in this figure legend, the reader is referred to the web version of this article.)

employed image cubic spline interpolation so that DIR was applied to images of the same resolution.

In addition, there are many possible expressions for the definition of elasticity, all of which are only surrogates for physical elasticity which requires knowledge of applied forces that cannot be determined from images. While a value greater or less than 1 indicates MPN volume ratio greater or less than the surrounding ring, as seen in Fig. 4, this results in a distribution that is skewed. An alternative formulation such as $(log\frac{\varphi_{DIR_{MPN}}}{\varphi_{DIR_{Ring}}})$ might be more physically intuitive since expansion or compression would have symmetrical effects but with opposite sign about zero. Such formulations may be helpful to explore in future studies.

To the best of our knowledge, this is the first study to calculate the elasticity of MPN from dynamic thoracic CT images. This provides the technical framework for testing the hypothesis that MPN and benign pulmonary nodule differ in elasticity. This difference may come from increased interstitial fluid pressure in tumors which can change the elasticity of MPN prior to any changes in morphological features. Studies have shown that most solid tumors have increased interstitial fluid pressure. This has been shown for breast carcinoma [2,3], metastatic melanoma [4,5], head and neck carcinoma [6], and colorectal carcinoma [2], with values as high as 60 mmHg. The tumor interstitial fluid pressure is uniform throughout the center of the tumor and drops steeply in its periphery [21–23]. The mechanisms that determine the increased tumor interstitial fluid pressure are not fully understood, but are thought to involve blood-vessel leakiness, lymphatic vessel abnormalities, interstitial fibrosis and a contraction of the interstitial space mediated by stromal fibroblasts, all of which are hallmarks of cancer [24,25].

Since a limitation of current CT based screening for lung cancer is distinguishing malignant from benign nodule [26], our method could impact clinical practice by increasing the specificity of CT-based lung cancer screening. In addition CT elastometry may predict tumor aggressiveness that could potentially be used in multifocal lung cancer patients to ascertain and treat the most aggressive lesions first. Ultimately it may even be helpful to distinguish aggressiveness of different tumor regions to guide radiation therapy dose painting or adaptive boost design.

Future directions include applying our analysis to both proven malignant and benign nodules, and ultimately may differentiate the aggressiveness of tumors or tumor regions to aid radiation therapy target selection or dose painting [27]. We will also evaluate nodule deformation homogeneity using strain tensors map, to determine whether this information could aid in distinguishing between malignant and non-malignant nodules. In addition we will attempt to extend our method to 4D CT images routinely acquired for radiotherapy simulation.

In conclusion, we developed a noninvasive method based on DIR of inhale/exhale breath-hold images to determine MPN elasticity.

Conflict of interest

None.

Acknowledgment

This study has been supported by Department of Defense LCRP 2011 #W81XWH-12-1-0286.

Appendix A. Supplementary data

Supplementary data associated with this article can be found, in the online version, at http://dx.doi.org/10.1016/j.radonc.2015.03.015.

References

[1] Sayyouh M, Vummidi DR, Kazerooni EA. Evaluation and management of pulmonary nodules: state-of-the-art and future perspectives. Expert Opin Med Diagn 2013;7:629–44.
[2] Less JR, Posner MC, Boucher Y, Borochovitz D, Wolmark N, Jain RK. Interstitial hypertension in human breast and colorectal tumors. Cancer Res 1992;52:6371–4.
[3] Nathanson SD, Nelson L. Interstitial fluid pressure in breast cancer, benign breast conditions, and breast parenchyma. Ann Surg Oncol 1994;1:333–8.
[4] Boucher Y, Kirkwood JM, Opacic D, Desantis M, Jain RK. Interstitial hypertension in superficial metastatic melanomas in humans. Cancer Res 1991;51:6691–4.
[5] Curti BD, Urba WJ, Alvord WG, et al. Interstitial pressure of subcutaneous nodules in melanoma and lymphoma patients: changes during treatment. Cancer Res 1993;53:2204–7.
[6] Gutmann R, Leunig M, Feyh J, et al. Interstitial hypertension in head and neck tumors in patients: correlation with tumor size. Cancer Res 1992;52:1993–5.
[7] Yin M, Talwalkar JA, Glaser KJ, et al. Assessment of hepatic fibrosis with magnetic resonance elastography. Clin Gastroenterol Hepatol 2007;5:1207–13.
[8] Venkatesh SK, Yin M, Ehman RL. Magnetic resonance elastography of liver: technique, analysis, and clinical applications. J Magn Reson Im 2013;37:544–55.
[9] Dice LR. Measures of the amount of ecologic association between species. Ecology 1945;26:297–302.
[10] Riegel AC, Chang JY, Vedam SS, Johnson V, Chi P-CM, Pan T. Cine Computed tomography without respiratory surrogate in planning stereotactic radiotherapy for non-small-cell lung cancer. Int J Radiat Oncol Biol Phys 2009;73:433–41.
[11] Nie K, Chuang C, Kirby N, Braunstein S, Pouliot J. Site-specific deformable imaging registration algorithm selection using patient-based simulated deformations. Med Phys 2013;40:041911.

[12] Wu J, Lei P, Shekhar R, Li H, Suntharalingam M, D'Souza WD. Do Tumors in the lung deform during normal respiration? an image registration investigation. Int J Radiat Oncol Biol Phys 2009;75:268–75.
[13] Liu X, Saboo RR, Pizer SM, Mageras GS. A shape-navigated image deformation model for 4D lung respiratory motion estimation. IEEE Int Symp Biomed Imaging 2009:875–8.
[14] Reinhardt JM, Ding K, Cao K, Christensen GE, Hoffman EA, Bodas SV. Registration-based estimates of local lung tissue expansion compared to xenon-CT measures of specific ventilation. Med Image Anal 2008;12:752–63.
[15] Negahdar M, Amini AA. Regional lung strains via a volumetric mass conserving optical flow model. IEEE International Symposium on Biomedical Imaging (ISBI): From Nano to Macro; Barcelona, Spain: 2012.
[16] Negahdar M, Amini AA. Tracking planar lung motion in 4D CT with optical flow: validations and comparison of global, local, and local-global methods. Medical Imaging 2010: Biomedical Applications in Molecular, Structural, and Functional Imaging; San Diego, CA, USA 2010;7626-74.
[17] Chaojie Z, Xiuying W, Jinhu C, Yong Y, Dagan F. Deformable registration model with local rigidity preservation for radiation therapy of lung tumor. Image Processing (ICIP), 2012 19th IEEE International Conference on:2012:1673–6.
[18] van Dam IE, van Sörnsen de Koste JR, Hanna GG, Muirhead R, Slotman BJ, Senan S. Improving target delineation on 4-dimensional CT scans in stage I NSCLC using a deformable registration tool. Radiother Oncol 2010;96:67–72.
[19] Speight R, Sykes J, Lindsay R, Franks K, Thwaites D. The evaluation of a deformable image registration segmentation technique for semi-automating internal target volume (ITV) production from 4DCT images of lung stereotactic body radiotherapy (SBRT) patients. Radiother Oncol 2011;98:277–83.
[20] Negahdar M, Dunlap N, Zacarias A, Eivelek AC, Woo SY, Amini AA. Strain as a novel index of regional pulmonary function from thoracic 4D CT images: in-vivo validation with tomographic SPECT ventilation and perfusion. Medical Imaging 2013: Biomedical Applications in Molecular, Structural, and Functional Imaging; Orlando, FA, USA 2013; 8672-38.
[21] Boucher Y, Baxter LT, Jain RK. Interstitial pressure gradients in tissue-isolated and subcutaneous tumors: implications for therapy. Cancer Res 1990;50:4478–84.
[22] DiResta GR, Lee J, Larson SM, Arbit E. Characterization of neuroblastoma xenograft in rat flank. I. Growth, interstitial fluid pressure, and interstitial fluid velocity distribution profiles. Microvasc Res 1993;46:158–77.
[23] Eikenes L, Bruland ØS, Brekken C, Davies CdL. Collagenase increases the transcapillary gradient and improves the uptake and distribution of monoclonal antibodies in human osteosarcoma xenografts. Cancer Res 2004;64:4768–73.
[24] Heldin CH, Rubin K, Pietras K, Ostman A. High interstitial fluid pressure – an obstacle in cancer therapy. Nat Rev Cancer 2004;4:806–13.
[25] Sarntinoranont M, Rooney F, Ferrari M. Interstitial stress and fluid pressure within a growing tumor. Ann Biomed Eng 2003;31:327–35.
[26] Aberle DR, Adams AM, Berg CD, et al. Reduced lung-cancer mortality with low-dose computed tomographic screening. N Engl J Med 2011;365:395–409.
[27] Maldonado F, Boland JM, Raghunath S, et al. Non-invasive Characterization of the Histopathologic Features of Pulmonary Nodules of the Lung Adenocarcinoma Spectrum using Computer Aided Nodule Assessment and Risk Yield (CANARY) – a Pilot Study. J Thorac Oncol 2013;8:452–60.